Disentangling the Drivers of the Ozone-Temperature Relationship over the United States

Gaige Hunter Kerr[1], Darryn W. Waugh[1,2], Sarah A. Strode[3,4], Stephen D. Steenrod[3,4], Luke D. Oman[4], and Susan E. Strahan[3,4]

[1]Department of Earth & Planetary Sciences, Johns Hopkins University, Baltimore, MD, USA
[2]School of Mathematics, University of New South Wales, Sydney, New South Wales, Australia
[3]Universities Space Research Association (USRA), GESTAR, Columbia, MD, USA
[4]NASA Goddard Space Flight Center, Greenbelt, MD, USA

Key Points:

- The GMI CTM reproduces the large-scale distribution of O_3 and the covariance of O_3 with temperature
- In regions where the O3-temperature correlation is strongly positive, transport drives the O_3-temperature relationship
- Future changes of dO_3/dT are uncertain due to the indirect association of O_3 and transport

Corresponding author: Gaige Hunter Kerr, gaige.kerr@jhu.edu

Abstract

Summertime surface-level ozone (O_3) is known to vary with temperature, but the relative roles of different processes responsible for causing the O_3-temperature relationship are not well quantified. In this study we use simulations of NASA's Global Modeling Initiative (GMI) chemical transport model (CTM) to isolate and assess the relative impact of atmospheric transport, chemistry, and emissions on O_3 variability, events, and its correlation with temperature. Using observations from CASTNet in the contiguous United States, we show that the GMI CTM reproduces the spatiotemporal variability of O_3 and the O_3-temperature relationship during the summer. We primarily focus on the total change in O_3 due to a change in temperature (dO_3/dT). In regions with strong positive correlations between temperature and O_3 such as the Northeast, Great Lakes, and Great Plains, temperature's association with transport primarily drives dO_3/dT with smaller contributions from temperature-dependent chemistry and anthropogenic emissions. There are regions, however, with near-zero correlation between temperature and O_3, and our findings suggest that transport is still an important driver of O_3 variability in these regions, albeit not correlated with temperature. Transport is not directly dependent on temperature but rather is linked through an indirect association, and it is therefore important to understand the exact mechanisms that link transport to O_3 and how these mechanisms will change in a warming world.

1 Introduction

It is well-established that high concentrations of surface-level ozone (O_3) coincide with high temperature (e.g., Bloomer et al., 2009; Schnell & Prather, 2017; Kerr & Waugh, 2018). This relationship is often quantified by the slope of the linear regression of O_3 versus temperature, herein referred to as "dO_3/dT." The observed dO_3/dT in the United States (U.S.) generally ranges from 0-6 ppbv K^{-1}, with higher values found (1) in the Northeastern compared to the Southeastern U.S. (e.g., Rasmussen et al., 2012; Brown-Steiner et al., 2015), (2) in urban regions (e.g., Sillman & Samson, 1995), and (3) during periods with higher anthropogenic nitrogen oxides ($NO_x \equiv NO + NO_2$) emissions (e.g., Bloomer et al., 2009; Rasmussen et al., 2012, 2013).

By virtue of the coincidence of O_3 and temperature, some have raised the possibility of a warming planet worsening O_3 pollution irrespective of changes in emissions or other human activities. This idea has been termed the "climate penalty," or variations thereof, and is most often quantified by dO_3/dT (Wu et al., 2008; Bloomer et al., 2009; Rasmussen et al., 2012; He et al., 2013; Rasmussen et al., 2013; Pusede et al., 2015; Jing et al., 2017). However, a wide range of processes influences O_3 and dO_3/dT, and

these processes may not respond uniformly to future changes in the climate. On account of this, it is important to understand the processes responsible for $d\mathrm{O_3}/d\mathrm{T}$, their relative roles in order to interpret the variability and historical trends of $\mathrm{O_3}$ in light of emission reductions (e.g., He et al., 2013; de Gouw et al., 2014; Simon et al., 2015), and how future changes in the climate system will affect $d\mathrm{O_3}/d\mathrm{T}$.

The process comprising $d\mathrm{O_3}/d\mathrm{T}$ can be cast in a general form as the sum of partial derivatives (Rasmussen et al., 2012):

$$\frac{d\mathrm{O_3}}{d\mathrm{T}} = \sum_i \frac{\partial \mathrm{O_3}}{\partial F_i} \frac{\partial F_i}{\partial \mathrm{T}}, \tag{1}$$

where T is temperature and F_i refers to a process that is temperature dependent or associated with temperature. One example of F_i is chemical reactions: an increase in temperature typically increases reactivity and thereby affects the production and lifetimes of $\mathrm{O_3}$, its precursor species, and its sinks (Jacob et al., 1993; Sillman & Samson, 1995; Pusede et al., 2015). The emission of $\mathrm{O_3}$ precursors such as isoprene, monoterpenes, and other biogenic volatile organic compounds (VOC) represent another F_i as their emission rates depend on ambient temperature (Sillman & Samson, 1995; Jacob & Winner, 2009; Pusede et al., 2015). Although often overlooked, anthropogenic NO_x emissions are also dependent on temperature, with an increase on hot days due to increased electricity demand for air conditioning (He et al., 2013; Abel et al., 2017).

Both vertical and horizontal transport are other examples of F_i, although not direct dependencies in the same vein as kinetics or emissions. Variations in transport are inexorably associated with temperature variability and ultimately influence the ability of $\mathrm{O_3}$ and its precursors to accumulate under conditions amenable for photochemistry. Horizontal transport impacts $\mathrm{O_3}$ through antecedent meteorological conditions ranging from frontal passages on mesoscales to stagnating high pressure systems on synoptic scales (Leibensperger et al., 2008; Barnes & Fiore, 2013; Fiore et al., 2015). With respect to vertical transport, planetary boundary layer (PBL) dynamics affect the entrainment and dilution of polluted air (Sillman & Samson, 1995), and dry deposition, the dominant sink for ozone in most of the continental surface layer (Kavassalis & Murphy, 2017), varies with temperature (Wesely, 1989).

While $d\mathrm{O_3}/d\mathrm{T}$ can be easily elicited from observations, disentangling the individual processes comprising this total derivative (Equation 1) is empirically more difficult. Previous studies have examined the role of different processes linking $\mathrm{O_3}$ with temperature, but there is no general consensus on the relative roles of the drivers of the $\mathrm{O_3}$-temperature relationship. For example, Jacob et al. (1993) used model simulations over the continental U.S. with and without fixed temperature and determined that while a part of the $\mathrm{O_3}$-

temperature relationship reflected the association of high temperature with stagnation, most of the temperature dependence could be attributed to chemistry, mainly to the storage of NO_x by peroxyacetyl nitrate (PAN) at low temperature but also to the association of high temperature with stagnation. Using emissions data from the 1990s and 2000s and observations from the DISCOVER-AQ campaign in 2011, He et al. (2013) estimated that one-third of $d\mathrm{O_3}/d\mathrm{T}$ is attributable to temperature-dependent anthropogenic NO_x emissions in the Mid-Atlantic U.S. Pusede et al. (2015) synthesized observations and modeling studies from around the U.S. to suggest that trends in $d\mathrm{O_3}/d\mathrm{T}$ imply chemistry, not meteorology, controls $d\mathrm{O_3}/d\mathrm{T}$, and further NO_x reductions in NO_x-limited regions will cause $d\mathrm{O_3}/d\mathrm{T}$ will reach a minimum in the future. Jing et al. (2017) reported that NO_x emission reductions were less effective at reducing $d\mathrm{O_3}/d\mathrm{T}$ in the Midwestern U.S. during the 2000s and 2010s compared to the 1990s. These contradictory results motivate this study to systematically examine the drivers of the O_3-temperature relationship.

In this paper we combine observations together with simulations using a CTM to isolate pathways that link temperature to transport, chemistry, and anthropogenic emissions. Sensitivity simulations are performed to examine the roles of these different pathways on O_3 variability, extremes, and its relationship with temperature over the contiguous U.S.

Section 2 describes NASA's Global Modeling Initiative (GMI) chemistry and transport model (CTM), observations, and our statistical approach to evaluating results. We first evaluate the performance of the CTM against observations and demonstrate that the CTM captures the main features of surface-level O_3, its extremes and variability, and its relationship with temperature over the contiguous United States (Section 3). Sections 4 and 5 show results across the Northeastern U.S. and contiguous U.S., respectively, and we discuss the role of anthropogenic NO_x emissions on O_3 in light of observed precursor emissions reductions (Section 4.1).

2 Data and Methodology

2.1 Observations

We use hourly O_3 observations from the Clean Air Status and Trends Network (CASTNet) for summers (1 June - 31 Aug; JJA) 2008-2010 at 78 sites across the contiguous U.S., shown in Figure 1. These summers reflect a period during which NO_x emissions and O_3 have stabilized across the Eastern U.S. following drastic reductions in NO_x emissions due to regulatory measures (He et al., 2013). Additional discussion on CASTNet history, monitor siting, and site relocations can be found in Cooper et al. (2012).

We obtain surface-level (2-meter) temperature from the Modern-Era Retrospective analysis for Research and Applications, Version 2 (MERRA-2; Gelaro et al., 2017) for the analysis of the O_3-temperature relationship and abbreviate it as "T" in figures, tables, and equations. The MERRA-2 reanalysis is also used to drive the CTM used in this study (see Section 2.2) and has shown to be in good agreement with observations in the mid-latitudes and an improvement over MERRA-1 (Bosilovich, 2015). When we compare MERRA-2 temperature with O_3 observations, we sample temperature at grid cells co-located with CASTNet sites (Figure 1). For consistency, we also use MERRA-2 temperature to examine the O_3-temperature relationship within the CTM. When we do this, we interpolate the MERRA-2 data from their native resolution (0.5° latitude $\times$ 0.625° longitude) to the coarser resolution of the CTM using cubic splines.

Anthropogenic NO_x emissions from stationary industrial sources (e.g., power plants, factories) are measured by the EPA Continuous Emissions Monitoring Systems (CEMS). We consider daily cumulative NO_x emissions recorded at these stationary sources, here shown in Figure S1.

2.2 Model Description and Simulations

Our primary tool for disentangling the drivers of the O_3-temperature relationship is simulations of the GMI CTM. Meteorological fields from MERRA-2 are provided to the CTM every 3 hours (Goldberg et al., 2017). Our simulations have a spatial resolution of 1° latitude $\times$ 1.25° longitude (Figure 1). The 72 level hybrid vertical coordinate is terrain-following for the first 31 levels (σ), changing to true pressure at 164 hPa. Seven model levels lie below 900 hPa ($\sim$ 1 km); and, in this study, we use output from the lowest model level, which has a thickness of $\sim$ 130 m. The model's stratosphere-troposphere chemical mechanism contains roughly 120 gas phase species and simulates over 400 reactions, including heterogeneous chemical reactions (Strahan et al., 2007; Duncan et al., 2007; Strahan et al., 2013).

Emissions of CO, NO, and non-methane VOC vary on monthly or interannual bases and are derived from the Emissions Database for Global Atmospheric Research (EDGAR) 3.2 inventory (Olivier et al., 2005). The EDGAR inventory is overwritten with regional inventories (e.g., NEI, CAC, EMEP, etc.) when applicable, and annual scaling factors are applied from the GEOS-Chem CTM. Isoprene emissions depend on climatological leaf area index, temperature, and photosynthetically active radiation and are calculated online via the Model of Emissions of Gases and Aerosols from Nature (MEGAN) (Guenther et al., 1995, 2012). Soil NO_x emissions, dependent upon temperature and precipitation, are also calculated online (Yienger & Levy, 1995).

The GMI CTM outputs O_3 at overpass time of the Afternoon Constellation ("A-Train") of Earth-observing satellites (mean 1300-1400 hours local time, "overpass2" in `https://modelingguru.nasa.gov/docs/DOC-2313`) for every grid cell on the globe, whereas hourly output is only provided at specific sites. We use model output at this overpass time, allowing us to conduct a more comprehensive spatial analysis than could be conducted with the hourly output. The early afternoon, the time of satellite overpass, generally coincides with peak daily O_3 concentrations (Fiore, 2002). We also average hourly observations from CASTNet over the same hours (1300-1400 hours local time) for validation of the CTM at locations of CASTNet sites. We refer to model output and observations from this time as "afternoon" throughout this manuscript.

We compare modeled and observed O_3 at overpass time to the same quantities from hourly output averaged over 1100-1600 hours local time after Strode et al. (2015), and we find that both temporal averaging approaches yield comparable model-observation agreement and variability. For the summer of 2010, O_3 averaged over 1100-1600 hours at sites with hourly output in the Northeastern U.S. is generally within ~ 5 ppbv of O_3 at overpass time averaged over grid cells in the region (Figure S2). We find no appreciable spatial pattern in the bias (not shown).

We conduct three GMI CTM sensitivity simulations spanning summers 2008-2010 that isolate the influences of the three main groups of processes controlling $d\mathrm{O}_3/d\mathrm{T}$: transport, chemistry, and emissions (Section 1). Our approach to fix temperature as it pertains to certain processes within the CTM is similar to Jacob et al. (1993), but here we use a CTM that has several improvements over theirs (e.g., high horizontal and vertical resolution, global coverage, driven by meteorological reanalyses for direct comparison with observations).

Transport: In this sensitivity simulation, the daily temperature dependence of chemical kinetics, radiation, cloud fields, and natural and anthropogenic emissions is removed ($\partial F_i/\partial \mathrm{O}_3 = 0$) such that temperature inputs derive from a monthly mean diurnal temperature curve, and emissions vary only from month to month (Table 1). As a result, the only processes that have daily variability and an association with temperature on sub-daily and daily timescales are transport by wind components, convective mass flux, PBL height, loss processes, pressure, and vertical mixing (Table 1).

+Chemistry: This second sensitivity simulation is the same as the Transport simulation except it also includes the daily variability of temperature-dependent, chemistry-related fields (Table 1). Although we denote this simulation as "+Chemistry" for brevity, these daily-varying, chemistry-related fields include more than just kinetics but also all

input variables to the chemical mechanism (e.g., temperature, cloud fraction, albedo, etc.) and processes embedded in the mechanism (e.g., reaction rates, photolysis, biogenic emissions, etc.). This simulation is identical to the simulation used in Douglass et al. (2017) but at higher resolution. Additional details can be found under "HindcastMR2" at `https://gmi.gsfc.nasa.gov/merra2hindcast/`.

+AEmissions: The third and final sensitivity simulation focuses on the role of temperature-dependent, anthropogenic NO_x emissions (Table 1). The first two sensitivity simulations (Transport and +Chemistry) have only monthly mean NO emissions from anthropogenic sources, but in the +AEmissions simulation we add daily variability to these emissions with the observed relationship between industrial NO_x emissions and temperature. It is important to note that although we examine the relationship between observed industrial NO_x emissions and temperature, the CTM's emissions inventory contains only NO emissions (as NO_x is primarily emitted as NO).

We consider the impact of NO_x emissions by perturbing the CTM's NO emissions. Daily variations are added in such a way that the monthly averages of the daily-varying NO emissions in the +AEmissions ($\mathrm{NO}_{\mathrm{CTM}}(t)$) are equal to the monthly mean NO emissions ($\overline{\mathrm{NO}_{\mathrm{CTM}}}$) in the Transport and +Chemistry simulations; specifically,

$$\mathrm{NO}_{\mathrm{CTM}}(t) = \overline{\mathrm{NO}_{\mathrm{CTM}}}[1 + \zeta \cdot \mathrm{T}(t)], \tag{2}$$

where ζ is the sensitivity of industrial NO_x emissions to temperature. To calculate ζ, we use CEMS data from the Eastern U.S. and define the sensitivity as

$$\zeta = \frac{\partial \widehat{\mathrm{NO}}_{x,\,\mathrm{CEMS}}(t)}{\partial \mathrm{T}(t)}, \tag{3}$$

where $\widehat{\mathrm{NO}}_{x,\,\mathrm{CEMS}}(t)$ are daily industrial NO_x emissions normalized by their monthly mean values. We calculate ζ for 26 states in the Eastern U.S. and the District of Columbia and find that ζ ranged from 2.6% K^{-1} (Tennessee) to 15.0% K^{-1} (Connecticut) during the 2000s. Averaged over the entire Eastern U.S. $\zeta = 5.6\%\ \mathrm{K}^{-1}$. Our results are consistent with other CEMS NO_x-temperature sensitivities reported in the literature: He et al. (2013) determined sensitivities in the range of 2.5-4.0% K^{-1} for five states in the Mid-Atlantic U.S., and Abel et al. (2017) found a sensitivity of 3.6% K^{-1} in the Eastern U.S. As industrial NO_x emissions contribute $\sim 60\%$ to total ambient NO_x concentrations (He et al., 2013), we perturb this percent of the NO in the emissions inventory. In our +AEmissions simulation we apply our regionally-averaged sensitivity (i.e., 5.6% K^{-1}) to the shaded region in the inset map in Figure 2. Figure 2 illustrates how this sensitivity simulation's emissions inventory is temperature dependent compared to the emissions inventory for the +Chemistry simulation.

2.3 Metrics

We examine several different measures of the O_3-temperature relationship in both observations and our sensitivity simulations.

We use the Pearson product-moment correlation coefficient (r) to assess the temporal correlation between simulations and observations. We define dO_3/dT as the slope of the Ordinary Least Squares (OLS) linear regression of O_3 against temperature. In this study we use dO_3/dT to (1) evaluate the performance of the GMI CTM by examining the sensitivity of modeled O_3 to changes in temperature against the observed sensitivity and (2) quantify the relative differences in the sensitivity of O_3 to temperature between our simulations. Determining dO_3/dT with OLS is the most common approach in the literature (e.g. Bloomer et al., 2009; Rasmussen et al., 2012; Barnes & Fiore, 2013; Strode et al., 2015; Romer et al., 2018; Meehl et al., 2018) and allows us to compare our results with previous studies.

Differences between simulations are also examined in terms of the impact they have on days with extreme temperatures and O_3 concentrations. Similar to recent studies (e.g., Schnell & Prather, 2017; Sun et al., 2017; Kerr & Waugh, 2018), we define extremes in terms of exceedances above percentile thresholds. We adopt the 10^{th} and 90^{th} percentiles (P_{10} and P_{90}, respectively) as the thresholds for extreme O_3 and temperature events on both sides of the distributions, and we calculate the average O_3 concentration on days falling above (below) P_{90} (P_{10}). Specifically we examine the enhancement (reduction) of O_3 on event days, and we define this as the difference between the average concentration on days exceeding (less than) the extreme threshold and days with median O_3 concentrations ($O_{3,\,P_{50}}$) or temperatures ($O_3(T_{P_{50}})$).

Our analysis is presented both in terms of a station-by-station or grid cell-by-grid cell basis and using regionally-averaged quantities. When we provide regionally averaged results, we first average O_3 and temperature over a given region and thereafter calculate r, dO_3/dT, or other metrics using these regionally-averaged quantities.

3 Model Evaluation

Before examining the results of our sensitivity simulations, we evaluate the CTM's representation of surface-level O_3 and its relationship with temperature. For this evaluation we use the +AEmissions simulation as this simulation includes all temperature dependencies considered in this study (Table 1) and, of our three simulations, should most closely mirror reality.

Observations show that the highest mean O_3 concentrations in the U.S. are found in Southern California and downwind regions, the Ohio River Valley, and Mid-Atlantic states while the lowest concentrations occur in the Pacific Northwest and Northern New England (Figure 1a). The CTM generally captures this spatial variability. There are, however, biases in the magnitude of O_3, with a high model bias in the Eastern U.S. and a low model bias in the West. The biases at individual CASTNet sites and their co-located CTM grid cell range from -27.917 ppbv to 12.124 ppbv (Figures 1b), and the mean bias in the Northeast (outlined region in Figure 1b) is 3.148 ppbv. The modeled high bias in the Eastern U.S. is consistent with previous studies using other CTMs. Other studies generally report a bias greater than 10 ppbv during the summer months and sometimes exceeding 30 ppbv with the exact magnitude of the bias dependent on the specific CTM used and the specific spatial domain considered (e.g. Fiore et al., 2009; Rasmussen et al., 2012; Rieder et al., 2015; Brown-Steiner et al., 2015); yet, even at coarser resolutions, these CTMs are still capable of capturing synoptic-scale events (Fiore, 2003; Wu et al., 2008).

We next examine whether the model captures the observed O_3-temperature relationship across the U.S. Observed O_3 and temperature exhibit strong positive correlation (i.e., $r(\mathrm{T}, \mathrm{O_3}) > 0.6$) in a broad swath extending westward from the Northeast to the Great Plains and in California (Figure 3a). In regions with strong positive correlations, the coefficient of determination (r^2) indicates that $> 50\%$ of the variance of O_3 is explained by temperature. The observed correlation generally decreases with decreasing latitude, reaching a near-zero minimum in the Lower Mississippi River Valley (Figure 3a). Camalier et al. (2007) showed that temperature is no longer the leading meteorological variable explaining O_3 variability south of $\sim 35°$N, and humidity and transport become important in these regions. The cause of spatial variations in $r(\mathrm{T}, \mathrm{O_3})$ is beyond the scope of this study; however, Tawfik & Steiner (2013) and Kavassalis & Murphy (2017) found a similar transitional latitude and expounded on the roles of soil moisture and dry deposition on O_3 in detail.

The CTM generally reproduces the spatial pattern of daily $r(\mathrm{T}, \mathrm{O_3})$ present in observations, with strong positive correlations in the Northeast, Great Lakes, and Great Plains and near-zero correlations in the Southeast and Intermountainous West. However, the model has a tendency to slightly overestimate the magnitude of the correlation (Figure 3a). For instance, modeled $r(\mathrm{T}, \mathrm{O_3})$ is ~ 0.2 higher than observed values in the Ohio River Valley.

Next we compare $d\mathrm{O_3}/d\mathrm{T}$ from CASTNet with the CTM (Figure 3b). As with $r(\mathrm{T}, \mathrm{O_3})$, the CTM generally captures the high values of $d\mathrm{O_3}/d\mathrm{T}$ in the Northeast and Midwest

and the lower, near-zero values in the South and West. Both Rasmussen et al. (2012) and Strode et al. (2015) conducted similar analyses but during the 1990s and early 2000s, and we note similarities with respect to the spatial variability of $d\mathrm{O_3}/d\mathrm{T}$. Since the 1990s and early 2000s, our analysis for 2008-2010 shows that the magnitude of $d\mathrm{O_3}/d\mathrm{T}$ has declined throughout the domain, especially in the Southeastern U.S. (Figure 3b). Thus, our nationwide map of $d\mathrm{O_3}/d\mathrm{T}$ provides an update to these previous studies that focused on time periods preceding the passage of the NO_x State Implementation Plan (SIP) Call. Other studies report that $d\mathrm{O_3}/d\mathrm{T}$ will continue to decline and reach a minimum in the U.S. due to NO_x reductions resulting from regulatory measures (Pusede et al., 2015).

The range in the $\mathrm{O_3}$-temperature relationship across the contiguous U.S. (Figure 3) is also illustrated in Figure 4, which shows time series of temperature and $\mathrm{O_3}$ for four locations with varying degrees in the strength in the relationship. In Montana, Ohio, and California (Figure 4a-c), $r(\mathrm{T}, \mathrm{O_3})$ is equally strong, yet $d\mathrm{O_3}/d\mathrm{T}$ is nearly 50% less in Montana than in Ohio and is intermediate in California. Figure 4d demonstrates the anti-correlation of $\mathrm{O_3}$ and temperature common in the Southeastern U.S. and the subsequent negative values of $d\mathrm{O_3}/d\mathrm{T}$. The differences between the Transport and +Chemistry simulations at these locations will be further explored in Section 5.

Overall, our evaluation of the GMI CTM shows that despite biases that are consistent with other CTMs, the GMI CTM reproduces the large-scale distribution of $\mathrm{O_3}$ and the relationship of $\mathrm{O_3}$ with temperature, affirming its use as a tool to diagnose the drivers $d\mathrm{O_3}/d\mathrm{T}$ and $\mathrm{O_3}$ variability.

4 The Northeastern U.S.

As other studies have shown a strong positive correlation between $\mathrm{O_3}$ and temperature in the Northeastern U.S. (i.e., Rasmussen et al., 2012; Schnell & Prather, 2017; Kerr & Waugh, 2018), we first examine the drivers of the $\mathrm{O_3}$-temperature relationship using regionally-averaged quantities in this region (outlined region in Figure 1). As shown in Figure 5a and c, variations in regionally-averaged $\mathrm{O_3}$ are accompanied by similar variations in temperature in the Northeast. This results in a strong positive correlation coefficient ($r(\mathrm{T}, \mathrm{O_3}) = 0.783$) and a high $d\mathrm{O_3}/d\mathrm{T}$ of 1.553 ppbv K^{-1}, both calculated using regionally-averaged quantities. These results hold beyond the summer shown in Figure 5 (Kerr & Waugh, 2018).

As stated in Section 1, anthropogenic NO_x emissions are one possible driver of $\mathrm{O_3}$ variability. There are substantial daily variations in these emissions (Figure 5b). For instance, NO_x emissions are $\sim 25\%$ below their mean value in early July, and as temper-

atures in the Northeast increase (Figure 5a), the emissions increase, peaking around 50% of their mean value (Figure 5b). Thus, this represents a change of $\sim 75\%$ occurring over a period of only five days. The daily variability of NO_x emissions is correlated with temperature and O_3 ($r(NO_x, T) = 0.721$ and $r(NO_x, O_3) = 0.442$).

All sensitivity simulations capture the general timing of O_3 events present in observations resulting in strong positive correlations among each other (Northeast-averaged $r > 0.92$ for all combinations of the three simulations; Figure 5c). However, we note that the CTM misses some of the low O_3 events (Figure 5c). Similar behavior has been shown for other CTMs, such as GEOS-Chem (Travis et al., 2016).

The processes associated with temperature that are included in the Transport simulation achieve nearly 90% of the total daily variation present in the +AEmissions simulation ($r^2 = 0.861$). The changes in the correlation calculated between CASTNet and the different simulations of the CTM are small: $r(O_{3,\,\mathrm{CASTNet}}, O_{3,\,\mathrm{Transport}})$ increases from 0.667 to 0.767 when temperature-dependent chemistry is included in the +Chemistry simulation, but r slightly decreases in the +AEmissions simulation ($r(O_{3,\mathrm{CASTNet}}, O_{3,+\,\mathrm{Emissions}})$ = 0.756). While these values reflect only results from summer 2010, examining all summers in our three year measuring period leads to similar conclusions, and r calculated between CASTNet and different simulations does not change by more than 0.06 when comparing results from summer 2010 to the entire measuring period. These small differences in the correlations between CASTNet and the different CTM simulations are not statistically significant at the 0.01 level.

Next, we turn to dO_3/dT and how our sensitivity simulations change the magnitude of dO_3/dT (Figure 6). Our simulations generally agree with observations; and, as temperature dependencies are added, dO_3/dT is brought into closer agreement with observations. Figure 6b and c indicate a unimodal distribution for both temperature and O_3. Considering the association of transport with temperature alone yields dO_3/dT = 0.976 ppbv K^{-1} (Table 2). When temperature-dependent chemistry is included in the +Chemistry simulation, dO_3/dT increases to 1.549 ppbv K^{-1}. The inclusion of anthropogenic NO_x emissions (+AEmissions simulation) further increases dO_3/dT to 1.662 ppbv K^{-1}. Therefore, transport and chemistry have similar contributions to the full dO_3/dT (i.e., the difference between dO_3/dT in the +Chemistry and Transport simulations, 1.549 ppbv K^{-1} - 0.976 ppbv K^{-1} = 0.573 ppbv K^{-1}, is similar in magnitude to dO_3/dT from the Transport simulation; Table 2) while anthropogenic NO_x emissions play a small role.

The most obvious difference between simulations is the magnitude of O_3 extremes (Figure 5c). This is particularly evident during the multiday O_3 event occurring in early

July. At the beginning (1 July), Northeast-averaged O_3 concentrations are at their minimum value for the summer with a ~ 5 ppbv spread between simulations and the +AEmissions simulation having the lowest concentration. As the temperature rises (Figure 5a) and O_3 accumulates in the Northeastern U.S., all simulations miss the initial first peak recorded by CASTNet but capture the second peak on 7 July again with a ~ 5 ppbv spread between simulations and the +AEmissions simulation closest to observed values (Figure 5c).

The results from this example event hold for most other extreme O_3 events in our measuring period, and these extreme O_3 events largely coincide with extreme temperatures while mean O_3 concentrations remain nearly unchanged between simulations (μ in Table 2). If we systematically examine the enhancement of O_3 for high O_3 events ($O_{3,\,P_{90}} - O_{3,\,P_{50}}$ in Table 2), we find only a small spread (< 1 ppbv) between simulations. We note similar results for the other tail of the distribution ($O_{3,\,P_{10}} - O_{3,\,P_{50}}$ in Table 2). This small spread demonstrates that the Transport simulation with its invariant chemistry and emissions can still produce O_3 events of comparable magnitude to observed events.

The inclusion of temperature dependencies preferentially affects days with extreme temperatures, so it is no surprise that the largest difference between simulations occurs on hot days ($O_3(T_{P_{90}}) - O_3(T_{P_{50}})$ in Table 2) and cold days ($O_3(T_{P_{10}}) - O_3(T_{P_{50}})$ in Table 2) when all temperature dependencies are considered in the +AEmissions simulation. Additionally, as temperature dependencies are added from the Transport to +AEmissions simulations, there are successive increases in O_3 variability (σ in Table 2).

If we transform dO_3/dT from different CTM simulations, given in Table 2, to their percentage contribution to the full dO_3/dT from the +AEmissions simulation, we find that the Transport simulation contributes 58.7%, the +Chemistry simulation 34.5%, and the +AEmissions simulation 6.8% to the full dO_3/dT. This finding is consistent across other metrics in Table 2: for example, the Transport simulation contributes 55.4%, the +Chemistry simulation 36.8%, and the +AEmissions simulation 7.8% to the total enhancement of O_3 on hot days. Thus, the association of transport with temperature contributes $\sim 60\%$ of the variability and extremes while temperature-dependent chemistry and emissions contribute only $\sim 30\%$ and $\sim 10\%$, respectively.

4.1 The Role of Anthropogenic NO_x Emissions

Our analysis in the Northeastern U.S. suggests that the inclusion of temperature-dependent anthropogenic NO_x emissions are not a dominant driver of day-to-day variations in dO_3/dT or O_3 variability.

To further investigate our +AEmissions simulation, which focuses on daily variations in anthropogenic emissions, we turn to another modeling study that examined the interannual effects of anthropogenic emissions reductions through two GMI CTM simulations (Strode et al., 2015). This pair of simulations, which spans the measuring period 2000-2010, investigated long-term emission reductions in the Eastern U.S. and their effect on surface-level O_3. The first ("Standard," here abbreviated Std) is similar to our +Chemistry simulation but is driven by the MERRA-1 reanalysis (Rienecker et al., 2011) and uses a previous version of the CTM's chemical mechanism. The second simulation used in Strode et al. (2015) is the same as Std, but anthropogenic and biomass burning emissions are held at 2000 levels ("Emissions Fixed," here abbreviated EmFix). Comparing EmFix with Std provides a way to separate long-term reductions in emissions from other sources of variability, such as a changing climate. Additional details on model configuration and specifications can be found in Strode et al. (2015).

We quantify how changes within the CTM's emissions inventory alter NO_x and O_3 for (1) our +Chemistry and +AEmissions simulations and (2) for the Std and EmFix simulations in Strode et al. (2015) and find that the changes in O_3 and NO_x are consistent whether emissions are altered on daily timescales (this study) or on interannual timescales (Strode et al., 2015). In other words, the change in O_3 that we find on hot versus cold days between our +AEmissions and +Chemistry simulations is similar to the change over the course of a couple years of emissions reductions. Specifically, the effect of a 1 ppbv change in modeled NO_x on O_3 ($\frac{\Delta\, O_3}{\Delta\, NO_x}$) is $\sim$ 7.8 ppbv in our study and $\sim$ 9.0 ppbv in Strode et al. (2015) (Figure 7).

The real-world results of reductions in emissions bear a similar small change in O_3 (Figure 8). Despite average summertime CEMS NO_x reductions of $> 50\%$ in the Northeastern U.S. and similar trends of NO in the CTM's emissions inventory (Figure 8a), the summertime mean observed and modeled O_3 concentrations have decreased by substantially less, $\sim 10\%$ (8b). Large changes in emissions resulting in much smaller changes in O_3 was earlier suggested by Jacob et al. (1993) proposed a 50% reduction in NO_x emissions would only decrease O_3 levels by $\sim 15\%$ in the Eastern U.S., and this is broadly consistent with the $\sim 10\%$ role we found temperature-dependent anthropogenic emissions to have (Table 2).

The small effect we found temperature-dependent anthropogenic emissions to have on O_3 on daily timescales is also consistent with He et al. (2013) who suggested that approximately one-third of the increase of O_3 on hot days is due to anthropogenic emissions. Although the contribution we found from these emission is slightly smaller than their estimation, our analysis has the advantage of using a modeling framework that takes

into account non-linearity and daily variations among fields whereas the analysis of He et al. (2013) was based solely on time-averaged, linear relationships derived from observations.

5 Contiguous U.S.

We have shown the importance of temperature on processes related to transport and chemistry in the Northeast, and we now examine if this holds across the contiguous U.S. Given that the temperature-dependent anthropogenic NO emissions in the GMI CTM play only a small role in the Northeastern U.S. and generally contribute $< 10\%$ to the variability of O_3 and its relationship with temperature, we now focus only on the difference between the Transport and +Chemistry simulations. While our previous analysis used regionally-averaged quantities (Section 4), we next compare changes in several metrics between the Transport and +Chemistry simulations locally (at each grid cell).

As discussed in Section 3, the highest O_3 concentrations are generally found in industrial, populated regions (i.e., California, Ohio River Valley, and the Mid-Atlantic) and high elevation regions (i.e., Utah, Colorado, Arizona, New Mexico). Regions with strong positive $r(\mathrm{T}, \mathrm{O_3})$ and a high $d\mathrm{O_3}/d\mathrm{T}$ largely coincide with the highest O_3 concentrations in the contiguous U.S. (Figures 1a, 3). However, there are some regions of the U.S., such as parts of the Great Plains and Upper Midwest, which have moderate mean O_3 concentrations (~ 40 ppbv) but strong positive $r(\mathrm{T}, \mathrm{O_3})$ and a moderate $d\mathrm{O_3}/d\mathrm{T}$ (compare Figure 1 with Figure 3).

In Section 4 we quantified the roles of transport and chemistry on $d\mathrm{O_3}/d\mathrm{T}$ in the Northeastern U.S. and showed that the Transport simulation yielded the majority of the magnitude of the full $d\mathrm{O_3}/d\mathrm{T}$. A comparison of $d\mathrm{O_3}/d\mathrm{T}$ between the Transport and +Chemistry simulations across the contiguous U.S. reveals that regions with the highest $d\mathrm{O_3}/d\mathrm{T}$, such as the Northeast, Midwest, Great Plains, and California (Figure 3b), see only small reductions (generally $< 25\%$) in $d\mathrm{O_3}/d\mathrm{T}$ as temperature dependencies in the +Chemistry simulation are removed (Figures 4a-c, 9a-b). This indicates that transport-related processes are the dominant cause of the O_3-temperature relationship throughout much of the Northern U.S. (Figure 9c).

Small values (i.e., $< 50\%$) in Figure 9c suggest that a majority of the magnitude of $d\mathrm{O_3}/d\mathrm{T}$ results from the addition of temperature-dependent chemistry in the +Chemistry simulation. We see that these small values primarily occur in the southern half of the domain and particularly in the Southeastern U.S. The large purported role of chemistry-related processes in this region stems, in part, from the fact that there are weak (< 0.4)

correlations between temperature and O_3 (Figure 3a, 4d), denoted in Figure 9c by orange contours. Including temperature-dependent chemistry in the +Chemistry simulation does not affect the O_3-temperature relationship in the same manner as in regions with strong positive correlations.

Disregarding the regions where $r(\mathrm{T}, \mathrm{O_3}) < 0.4$, there are regions such as Virginia and North Carolina where $r(\mathrm{T}, \mathrm{O_3})$ is moderately positive, yet the magnitude of $d\mathrm{O_3}/d\mathrm{T}$ more than doubles as temperature-dependent chemistry is included (Figure 9a-b). This region coincides with higher isoprene emissions compared to the Northeast (not shown). The large role of chemistry in this Mid-Atlantic region could be the result of processes relevant to this region: the aforementioned isoprene (or other biogenic) emissions, the infrequent passage of cyclones south of $\sim 35°$N (Rasmussen et al., 2012), the influence of mesoscale processes not captured by the GMI CTM (e.g., land-sea breezes in coastal regions, recirculation). Further investigation is needed to understand how these processes might after O_3 in this region.

In the Northeast, we found that, on average, the magnitude of $\mathrm{O_{3,\ P_{90}}}$ changes by only < 2 ppbv between the +Chemistry and Transport simulations. As we expand our analysis to the contiguous U.S., we find that the Northeast, parts of California, and Gulf Coast states have the largest increase of O_3 for $\mathrm{O_{3,\ P_{90}}}$, generally > 10 ppbv with much more modest increases ($\sim$ 5 ppbv) in other regions (Figure 10a-b). Unlike the analysis of $d\mathrm{O_3}/d\mathrm{T}$ in Figure 9 where differences between simulations were largely a product of O_3-temperature correlations, the differences in the analysis of the increase of O_3 for $\mathrm{O_{3,\ P_{90}}}$ displays far greater spatial heterogeneity (Figure 10c). For instance, the Northeast, Midwest, and Great Plains are all regions with similar strong positive $r(\mathrm{T}, \mathrm{O_3})$, yet these regions do not respond uniformly as temperature-dependent chemistry is included. This is particularly evident for case studies shown in Figure 4a-b for Montana and Ohio. The O_3-temperature relationship is similar for both locations ($r(\mathrm{T}, \mathrm{O_3}) = 0.84$ in Ohio and $r(\mathrm{T}, \mathrm{O_3}) = 0.79$ in Montana), yet the Transport simulation provides nearly all the variability for the case of Montana (Figure 4a). Considering the association of temperature with transport alone in the Midwestern U.S. yields $\mathrm{O_{3,\ P_{90}}}$ of slightly larger magnitude, albeit only a $\sim 5\%$ increase (Figure 10c). In the Southeastern U.S., a region where $r(\mathrm{T}, \mathrm{O_3}) \approx 0$, the enhancement of O_3 for $\mathrm{O_{3,\ P_{90}}}$ implies that $\mathrm{O_{3,\ P_{90}}}$ have a greater magnitude when the temperature-dependent processes included in our +Chemistry simulation are held at their monthly mean values (Figure 10c).

We conduct a similar analysis to Figures 10 but for the reduction of O_3 for low O_3 events ($\mathrm{O_{3,\ P_{10}}}$; Figure S3). Comparing these two figures leads to qualitatively similar outcomes inasmuch as the Northeast and Mid-Atlantic states see the largest reductions

in O_3 for $O_{3,\,P_{10}}$ (Figure S3a-b). However, we note a general asymmetry between the change of O_3 for $O_{3,\,P_{90}}$ and $O_{3,\,P_{10}}$ (compare Figures 10 and S3) implying temperature-dependent chemistry makes a smaller difference for the upper tail of the O_3 distribution.

Similar to our analysis in Figure 10a-b showing the change of O_3 for O_3 events, we now turn to the change of O_3 for days with extreme temperatures. The Northeast stands out as the region with the largest O_3 enhancement on hot days (Figure 11a-b) and largest O_3 reduction on cold days (Figure S4a-b). In the Northeast, we found large changes between the Transport and +Chemistry simulations when we examined the increase of O_3 on hot days which implied that $\sim 60\%$ of this increase came about by considering only the association of temperature with transport-related processes. This holds throughout the northern portion of the domain, and we see that the processes included in our Transport simulation generally provide the majority of the total increase of O_3 for on hot days. The influence of transport's association with temperature diminishes with decreasing latitude reaching a minimum immediately north of the regions where $r(\mathrm{T}, \mathrm{O_3}) < 0.4$ (i.e., Northern California and Southern Oregon, Virginia and North Carolina). Here we note some of the largest changes between simulations, suggesting that the Transport simulation provides as little as 20% of the increase of O_3 on hot days (Figure 11c). Regions in which temperature and O_3 are weakly correlated ($r(\mathrm{T}, \mathrm{O_3}) < 0.4$) display sharp gradients between very large and very small ratios stemming from the quotient of two near-zero numbers. Again, we note an asymmetry in the effects of temperature dependencies on hot versus cold days (compare Figures 11 and S4).

In regions where $r(\mathrm{T}, \mathrm{O_3}) < 0.4$ such as the Southeastern U.S., transport still explains a majority of the variability of O_3. To illustrate this, we turn to a case study in Mississippi (Figure 4d). The difference between simulations throughout this region is often in the opposite direction of differences found elsewhere (i.e., the +Chemistry simulation reduces O_3 variability and extremes). These results are a manifestation of the lack of relationship between O_3 and temperature. As we have shown, the Northern U.S. and (to a lesser extent) California are generally defined by moderate to strong positive correlations along with a high $d\mathrm{O_3}/d\mathrm{T}$ (Figures 3, 4a-c) and the dominant role of transport (Figures 9-11, S3-S4). Thus, regardless of the strength of the relationship between O_3 and temperature, our comparison of the Transport and +Chemistry simulations in areas with high $r(\mathrm{T}, \mathrm{O_3})$ versus low r demonstrates that transport is the main driver of O_3 variability (Figures 4, 9-11, S3-S4).

6 Conclusions

We have found that the GMI CTM reproduces the large-scale distribution of O_3 and the O_3-temperature relationship. Both observed and modeled O_3 and temperature are strongly positively correlated throughout much of the northern U.S. with the highest correlations found in the Great Plains, Upper Midwest, Northeast, and California, but the relationship between O_3 and temperature is weak in the Southeastern U.S. (Figure 3a). The slope of the linear regression of O_3 versus temperature, $dO_3/d\mathrm{T}$, has similar spatial variability to $r(\mathrm{T}, O_3)$, but there are some differences: the highest values of $dO_3/d\mathrm{T}$ are located in the Midwest and Northeast while the magnitude of the slope diminishes to near-zero values in the Southeast and Intermountainous West.

In regions where O_3 and temperature have strong positive correlations, our analysis reveals the dominant role of transport on O_3. The processes included in our Transport simulation explain a majority ($\sim 60\%$) of O_3 variability and its coincidence with temperature and yield values of $dO_3/d\mathrm{T}$ that are comparable magnitude to observed quantities. On the other hand, temperature-dependent chemistry contributes $\sim 30\%$ to, for example, the full variability of O_3 or its relationship with temperature.

Even in regions with low correlations between O_3 and temperature (e.g., Southeastern U.S.), transport is still an important contributor to O_3 variability, although the variability resulting from transport is not associated with similar variations in temperature. Overall, regardless of the exact relationship between O_3 and temperature, the processes included in our Transport simulation play an important role in controlling O_3 variability.

In the Northeastern U.S. we found that anthropogenic emissions play a small role ($\sim 30\%$) with respect to O_3 events and the O_3-temperature relationship. While climate and air quality models include the impact of temperature on biogenic emissions and chemical processes, they do not include the impact of temperature on human behavior and anthropogenic emissions. Abel et al. (2017) have commented on this and called for an integration of the temperature dependence of anthropogenic NO_x into a modeling platform. Our present work does this and reveals that although the daily variability of anthropogenic NO_x emissions is large in term of its percent change (Figure 5b), the day-to-day changes are small in terms of the impact they have ambient NO_x and O_3 concentrations and their net effect on daily timescales is similar in magnitude to the changes that could be expected from long-term NO_x reductions over the course of one or two years.

Our findings suggest that temperature-dependent chemistry and anthropogenic emissions may be less important in controlling O_3 than previously thought (e.g., Jacob et al.,

1993; He et al., 2013; Romer et al., 2018). This is potentially important for the use of dO_3/dT as measure of how climate change may alter O_3 (or emission controls aimed at reducing O_3). Unlike photochemistry or emission pathways, the transport-temperature-O_3 pathway represents an indirect association; for example, a stagnating high pressure system is not directly dependent on temperature but generally coincides with high ambient temperatures. It is possible that this indirect association may change under a changing climate. While others have studied the roles of air mass type and origin, residence time, and mixing on O_3 (e.g., Samson & Ragland, 1977; Comrie, 1994; Davis et al., 2010), exactly how this transport and its relationship with temperature will change in a future climate is uncertain.

This points us to the important question of which aspect(s) of transport is responsible for O_3 variability and the O_3-temperature relationship. Embedded in our Transport simulation are many processes (i.e., PBL height (or mixing), deposition, synoptic-scale horizontal circulation, etc.) that all impact surface O_3, but it is unclear which of these processes dominates the transport-temperature-O_3 connection. While some work has explored how changes in large-scale transport could affect surface-level O_3 (e.g., Barnes & Fiore, 2013), it is not known exactly how many of the transport-related processes affecting O_3 will change in the future. Our future work will focus on quantifying the transport processes responsible for the O_3-temperature relationship, and how these processes might change in a warming world.

Acknowledgments

The CASTNet and CEMS datasets used in this study are publicly available at `epa.gov/castnet` and `ampd.epa.gov/ampd/`, respectively. The authors thank the EPA's Clean Air Markets Division for administering and operating the monitors and maintaining the datasets. GMI CTM data is accessible via anonymous FTP to `dirac.gsfc.nasa.gov` in the subdirectory /pub/gmidata2/. Author G. H. Kerr is supported by the National Science Foundation through the Water, Climate, and Health IGERT at Johns Hopkins University (#1069213).

References

Abel, D., Holloway, T., Kladar, R. M., Meier, P., Ahl, D., Harkey, M., & Patz, J. (2017). Response of power plant emissions to ambient temperature in the Eastern United States. *Environ. Sci. Technol.*, *51*(10), 5838–5846. doi: 10.1021/acs.est.6b06201

Barnes, E. A., & Fiore, A. M. (2013). Surface ozone variability and the jet posi-

tion: Implications for projecting future air quality. *Geophys. Res. Lett.*, *40*(11), 2839–2844. doi: 10.1002/grl.50411

Bloomer, B. J., Stehr, J. W., Piety, C. A., Salawitch, R. J., & Dickerson, R. R. (2009). Observed relationships of ozone air pollution with temperature and emissions. *Geophys. Res. Lett.*, *36*(9). doi: 10.1029/2009GL037308

Bosilovich, M.. G., Akella, A., Coy, L., Cullather, R., Draper, C., Gelaro, R., Kovach, R., Liu, Q., Molod, A., Norris, P., Wargan, K., Chao, W., Reichle, R., Takacs, L., Vikhliaev, Y., Bloom, S., Collow, A., Firth, S., Labow, G., Partyka, G., Pawson, S., Reale, O., Schubert, S.. D. & Suarez, M. (2015). *MERRA-2: Initial evaluation of the climate* (Tech. Rep. No. Volume 43).

Brown-Steiner, B., Hess, P., & Lin, M. (2015). On the capabilities and limitations of GCCM simulations of summertime regional air quality: A diagnostic analysis of ozone and temperature simulations in the US using CESM CAM-Chem. *Atmos. Environ.*, *101*, 134–148. doi: 10.1016/j.atmosenv.2014.11.001

Camalier, L., Cox, W., & Dolwick, P. (2007). The effects of meteorology on ozone in urban areas and their use in assessing ozone trends. *Atmos. Environ.*, *41*(33), 7127–7137. doi: 10.1016/j.atmosenv.2007.04.061

Comrie, A. C. (1994). Tracking ozone: Air-mass trajectories and pollutant source regions influencing ozone in Pennsylvania forests. *Ann. Am. Assoc. Geogr.*, *84*(4), 635–651. doi: 10.1111/j.1467-8306.1994.tb01880.x

Cooper, O. R., Gao, R.-S., Tarasick, D., Leblanc, T., & Sweeney, C. (2012). Long-term ozone trends at rural ozone monitoring sites across the United States, 1990-2010. *J. Geophys. Res.*, *117*(D22307). doi: 10.1029/2012JD018261

Davis, R. E., Normile, C. P., Sitka, L., Hondula, D. M., Knight, D. B., Gawtry, S. P., & Stenger, P. J. (2010). A comparison of trajectory and air mass approaches to examine ozone variability. *Atmos. Environ.*, *44*(1), 64–74. doi: 10.1016/j.atmosenv.2009.09.038

de Gouw, J. A., Parrish, D. D., Frost, G. J., & Trainer, M. (2014). Reduced emissions of CO_2, NO_x, and SO_2 from U.S. power plants owing to switch from coal to natural gas with combined cycle technology. *Earths Future*, *2*(2), 75–82. doi: 10.1002/2013EF000196

Douglass, A. R., Strahan, S. E., Oman, L. D., & Stolarski, R. S. (2017). Multi-decadal records of stratospheric composition and their relationship to stratospheric circulation change. *Atmos. Chem. Phys.*, *17*(19), 12081–12096. doi: 10.5194/acp-17-12081-2017

Duncan, B. N., Strahan, S. E., Yoshida, S. D., Steenrod, S. D. , & Livesey, N. (2007). Model study of cross-tropopause transport of biomass burning pollution.

Atmos. Chem. Phys., *7*, 3713–3736. doi: 10.5194/acp-7-3713-2007

Fiore, A. M. (2002). Background ozone over the United States in summer: Origin, trend, and contribution to pollution episodes. *J. Geophys. Res.*, *107*(D15). doi: 10.1029/2001JD000982

Fiore, A. M. (2003). Application of empirical orthogonal functions to evaluate ozone simulations with regional and global models. *J. Geophys. Res.*, *108*(D14). doi: 10.1029/2002JD003151

Fiore, A. M., Dentener, F. J., Wild, O., Cuvelier, C., Schultz, M. G., Hess, P., ... Zuber, A. (2009). Multimodel estimates of intercontinental source-receptor relationships for ozone pollution. *J. Geophys. Res.*, *114*(D4). doi: 10.1029/2008JD010816

Fiore, A. M., Naik, V., & Leibensperger, E. M. (2015). Air Quality and Climate Connections. *Journal of the Air & Waste Management Association*, *65*(6), 645–685. doi: 10.1080/10962247.2015.1040526

Gelaro, R., McCarty, W., Surez, M. J., Todling, R., Molod, A., Takacs, L., ... Zhao, B. (2017). The Modern-Era Retrospective Analysis for Research and Applications, Version 2 (MERRA-2). *J. Clim.*, *30*(14), 5419–5454. doi: 10.1175/JCLI-D-16-0758.1

Goldberg, D. L., Lamsal, L. N., Loughner, C. P., Swartz, W. H., Lu, Z., & Streets, D. G. (2017). A high-resolution and observationally constrained OMI NO_2 satellite retrieval. *Atmospheric Chem. Phys.*, *17*(18), 11403–11421.

Guenther, A., Hewitt, C. N., Erickson, D., Fall, R., Geron, C., Graedel, T., ... Zimmerman, P. (1995). A global model of natural volatile organic compound emissions. *J. Geophys. Res.*, *100*(D5), 8873. doi: 10.1029/94JD02950

Guenther, A. B., Jiang, X., Heald, C. L., Sakulyanontvittaya, T., Duhl, T., Emmons, L. K., & Wang, X. (2012). The Model of Emissions of Gases and Aerosols from Nature version 2.1 (MEGAN2.1): An extended and updated framework for modeling biogenic emissions. *Geosci. Model Dev.*, *5*(6), 1471–1492. doi: 10.5194/gmd-5-1471-2012

He, H., Hembeck, L., Hosley, K. M., Canty, T. P., Salawitch, R. J., & Dickerson, R. R. (2013). High ozone concentrations on hot days: The role of electric power demand and NO_x emissions: Ozone and power demand on hot days. *Geophys. Res. Lett.*, *40*(19), 5291–5294. doi: 10.1002/grl.50967

He, H., Stehr, J. W., Hains, J. C., Krask, D. J., Doddridge, B. G., Vinnikov, K. Y., ... Dickerson, R. R. (2013). Trends in emissions and concentrations of air pollutants in the lower troposphere in the Baltimore/Washington airshed from 1997 to 2011. *Atmos. Chem. Phys.*, *13*(15), 7859–7874. doi: 10.5194/acp-13-7859-2013

Jacob, D. J., Logan, J. A., Gardner, G. M., Yevich, R. M., Spivakovsky, C. M., & Wofsy, S. C. (1993). Factors Regulating Ozone Over the United States and Its Export to the Global Atmosphere. *J. Geophys. Res.*, *98*(D8), 14817–14826.

Jacob, D. J., & Winner, D. A. (2009). Effect of climate change on air quality. *Atmos. Environ.*, *43*(1), 51–63. doi: 10.1016/j.atmosenv.2008.09.051

Jing, P., Lu, Z., & Steiner, A. L. (2017). The ozone-climate penalty in the Midwestern U.S. *Atmos. Environ.*, *170*, 130–142. doi: 10.1016/j.atmosenv.2017.09.038

Kavassalis, S. C., & Murphy, J. G. (2017). Understanding ozone-meteorology correlations: A role for dry deposition: Ozone-Meteorology Correlations: Dry Dep. *Geophys. Res. Lett.*, *44*(6), 2922–2931. doi: 10.1002/2016GL071791

Kerr, G. H., & Waugh, D. W. (2018). Connections between summer air pollution and stagnation. *Environ. Res. Lett.*, *13*(8), 084001. doi: 10.1088/1748-9326/aad2e2

Leibensperger, E. M., Mickley, L. J., & Jacob, D. J. (2008). Sensitivity of US air quality to mid-latitude cyclone frequency and implications of 1980–2006 climate change. *Atmos. Chem. Phys.*, *8*(23), 7075–7086.

Meehl, G. A., Tebaldi, C., Tilmes, S., Lamarque, J.-F., Bates, S., Pendergrass, A., & Lombardozzi, D. (2018). Future heat waves and surface ozone. *Environ. Res. Lett.*, *13*(6), 064004. doi: 10.1088/1748-9326/aabcdc

Olivier, J. G. J., Van Aardenne, J. A., Dentener, F. J., Pagliari, V., Ganzeveld, L. N., & Peters, J. A. H. W. (2005). Recent trends in global greenhouse gas emissions:regional trends 19702000 and spatial distributionof key sources in 2000. *Environmental Sciences*, *2*(2-3), 81–99. doi: 10.1080/15693430500400345

Pitkänen, M. R. A., Mikkonen, S., Lehtinen, K. E. J., Lipponen, A., & Arola, A. (2016). Artificial bias typically neglected in comparisons of uncertain atmospheric data: Regression bias in atmospheric sciences. *Geophys. Res. Lett.*, *43*(18), 10,003–10,011. doi: 10.1002/2016GL070852

Pusede, S. E., Steiner, A. L., & Cohen, R. C. (2015). Temperature and Recent Trends in the Chemistry of Continental Surface Ozone. *Chem. Rev.*, *115*(10), 3898–3918. doi: 10.1021/cr5006815

Rasmussen, D., Fiore, A., Naik, V., Horowitz, L., McGinnis, S., & Schultz, M. (2012). Surface ozone-temperature relationships in the eastern US: A monthly climatology for evaluating chemistry-climate models. *Atmos. Environ.*, *47*, 142–153. doi: 10.1016/j.atmosenv.2011.11.021

Rasmussen, D. J., Hu, J., Mahmud, A., & Kleeman, M. J. (2013). The ozoneclimate penalty: Past, present, and future. *Environ. Sci. Technol.*, *47*(24), 14258–14266.

doi: 10.1021/es403446m

Rieder, H. E., Fiore, A. M., Horowitz, L. W., & Naik, V. (2015). Projecting policy-relevant metrics for high summertime ozone pollution events over the eastern United States due to climate and emission changes during the 21st century. *J. Geophys. Res.: Atmospheres*, *120*(2), 784–800.

Rienecker, M. M., Suarez, M. J., Gelaro, R., Todling, R., Bacmeister, J., Liu, E., ... Woollen, J. (2011). MERRA: NASAs Modern-Era Retrospective Analysis for Research and Applications. *J. Clim.*, *24*(14), 3624–3648. doi: 10.1175/JCLI-D-11-00015.1

Romer, P. S., Duffey, K. C., Wooldridge, P. J., Edgerton, E., Baumann, K., Feiner, P. A., ... Cohen, R. C. (2018). Effects of temperature-dependent NO_x emissions on continental ozone production. *Atmos. Chem. Phys.*, *18*(4), 2601–2614. doi: 10.5194/acp-18-2601-2018

Samson, P. J., & Ragland, K. W. (1977). Ozone and visibility reduction in the Midwest: Evidence for large-scale transport. *J. Appl. Meteorol. Climatol.*, *16*, 1101–1106. doi: https://doi.org/10.1175/1520-0450(1977)016⟨1101:AFWSIA⟩2.0.CO;2

Schnell, J. L., & Prather, M. J. (2017). Co-occurrence of extremes in surface ozone, particulate matter, and temperature over eastern North America. *Proc. Natl. Acad. Sci. U.S.A.*, *114*(11), 2854–2859. doi: 10.1073/pnas.1614453114

Sillman, S., & Samson, P. J. (1995). Impact on temperature on oxidant photochemistry in urban, polluted rural and remote environments. *J. Geophys. Res.*, *100*(D6), 11497–11508.

Simon, H., Reff, A., Wells, B., Xing, J., & Frank, N. (2015). Ozone Trends Across the United States over a Period of Decreasing NOx and VOC Emissions. *Environmental Science & Technology*, *49*(1), 186–195. doi: 10.1021/es504514z

Strahan, S. E., Duncan, B. N. & Hoor, P. (2007). Observationally derived transport diagnostics for the lowermost stratosphere and their application to the GMI. *Atmos. Chem. Phys.*, *7*, 2435–2445. doi: 10.5194/acp-7-2435-2007

Strahan, S. E., Douglass, A. R. & Newman, P. A. (2013). The contributions of chemistry and transport to low arctic ozone in March 2011 derived from Aura MLS observations. *J. Geophys. Res. Atmos.*, *118*(3), 1563–1576. doi: 10.1002/jgrd.50181

Strode, S. A., Rodriguez, J. M., Logan, J. A., Cooper, O. R., Witte, J. C., Lamsal, L. N., ... Strahan, S. E. (2015). Trends and variability in surface ozone over the United States. *J. Geophys. Res. Atmos.*, *120*(17), 9020–9042. doi: 10.1002/2014JD022784

Sun, W., Hess, P., & Liu, C. (2017). The impact of meteorological persistence on the distribution and extremes of ozone. *Geophys. Res. Lett.*, *44*, 1545–1553. doi: 10.1002/2016GL071731

Tawfik, A. B., & Steiner, A. L. (2013). A proposed physical mechanism for ozone-meteorology correlations using landatmosphere coupling regimes. *Atmos. Environ.*, *72*, 50–59. doi: 10.1016/j.atmosenv.2013.03.002

Travis, K. R., Jacob, D. J., Fisher, J. A., Kim, P. S., Marais, E. A., Zhu, L., ... Zhou, X. (2016). Why do models overestimate surface ozone in the Southeast United States? *Atmospheric Chem. Phys.*, *16*(21), 13561–13577. doi: 10.5194/acp-16-13561-2016

Wesley, M. L. (1989). Parameterization of surface resistances to gaseous dry deposition in regional-scale numerical models *Atmos. Environ.*, *23*(6), 1293–1304. doi: 10.1016/0004-6981(89)90153-4

Wu, S., Mickley, L. J., Leibensperger, E. M., Jacob, D. J., Rind, D., & Streets, D. G. (2008). Effects of 20002050 global change on ozone air quality in the United States. *J. Geophys. Res.*, *113*(D6). doi: 10.1029/2007JD008917

Yienger, J. J., & Levy, H. (1995). Empirical model of global soil-biogenic NO_x emissions. *J. Geophys. Res.*, *100*(D6), 11447. doi: 10.1029/95JD00370

768 **Table 1.** Summary of sensitivity simulations. We denote fields or processes with temperature
769 variability reduced to monthly mean values by ✗ and fields or process with daily temperature
770 variability by ✓.

	$\frac{\partial F_i}{\partial T} \neq 0$					
Simulation	**Transport**[a]	**Loss**[b]	**Reaction Rates**	**Radiation**[c]	**Natural Emissions**	**Anthropogenic Emissions**
Transport	✓	✓	✗	✗	✗	✗
+Chemistry	✓	✓	✓	✓	✓	✗
+AEmissions	✓	✓	✓	✓	✓	✓

[a] wind components, vertical mixing, convective mass flux, PBL height, pressure

[b] precipitation, wet and dry deposition

[c] clouds, aerosols, surface albedo

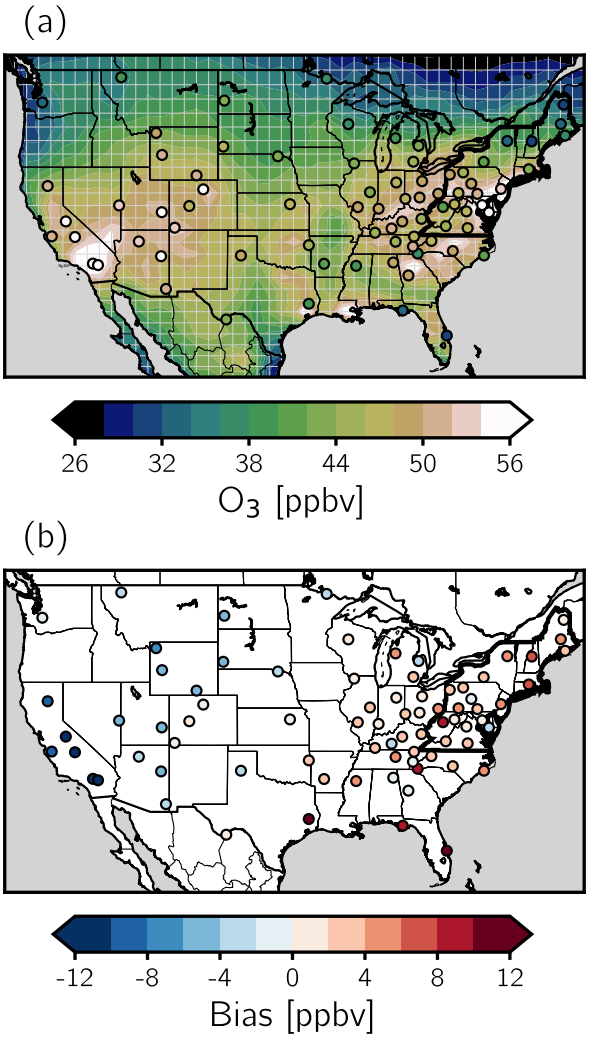

Figure 1. (a) Daily afternoon O_3 from observations (scatterpoints) and the +AEmissions simulation (contours) averaged over the measuring period, summers 2008–2010. The resolution of the CTM, 1.25° longitude × 1° latitude, is represented by the parallels and meridians, respectively. (b) Scatterpoints represent the O_3 bias (= CTM − CASTNet) of mean daily afternoon O_3 at individual CASTNet sites and their co-located CTM grid cell. Note the color scale saturates at −12 ppbv and 12 ppbv for better contrast. The Northeastern U.S. is outlined in black.

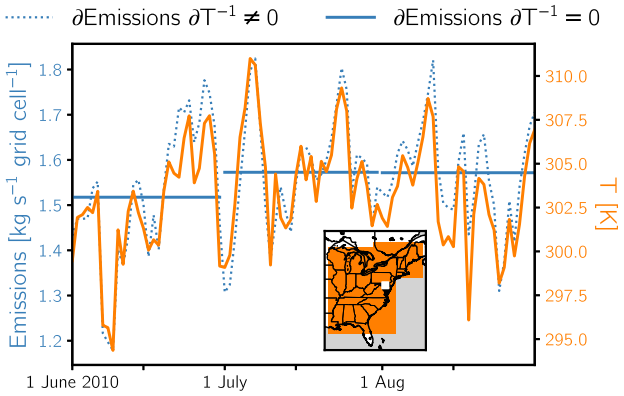

Figure 2. NO emissions from the emissions inventory of the +Chemistry simulation (solid blue) are shown alongside temperature-dependent NO emissions from the +AEmissions simulation (dashed blue) and temperature (T) for the CTM grid cell shown in white in the inset map. Temperature-dependent emissions are applied to all grid cells in the shaded region of the inset map in the +AEmissions simulation.

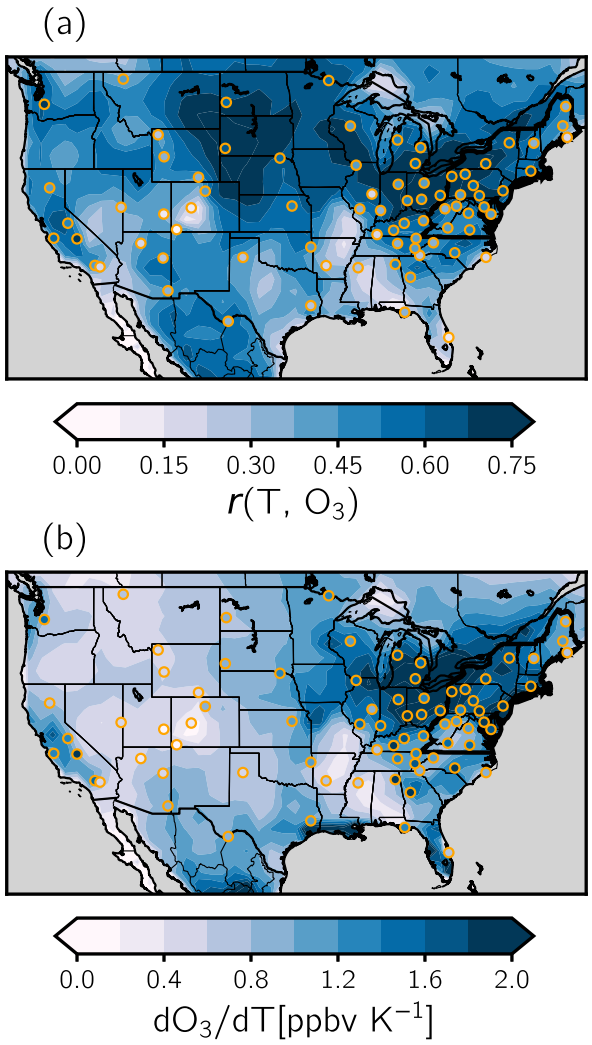

Figure 3. (a) Pearson product-moment correlation coefficients (r) and (b) the slope of the OLS linear regression ($d\mathrm{O_3}/d\mathrm{T}$) calculated between daily afternoon temperature and $\mathrm{O_3}$ for summers 2008-2010. Contours represent CTM output from the +AEmissions simulations, and orange outlined scatterpoints represent results from observations.

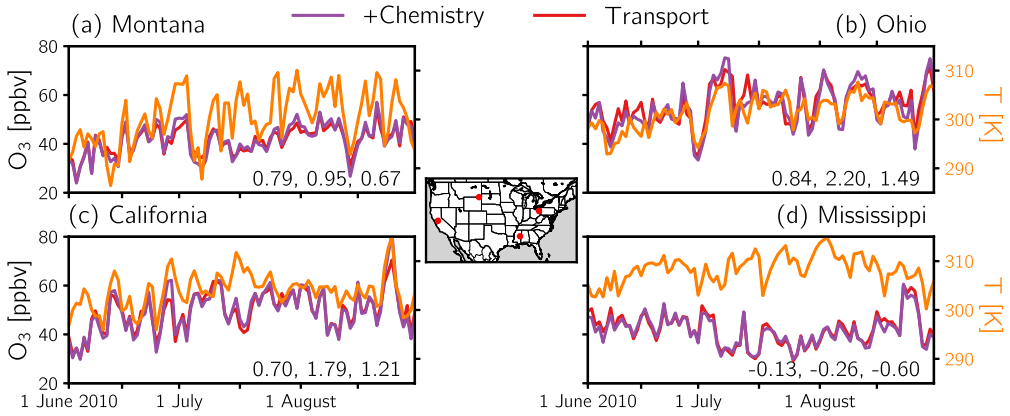

Figure 4. O_3 from the Transport and +Chemistry simulations and co-located temperature for summer 2010 for grid cells in regions with varying strength of the O_3-temperature relationship. The exact location of grid cells are shown in the inset map.

Text in the subplots' lower right corners indicate $r(\mathrm{T}, \mathrm{O}_{3,\,+\mathrm{Chemistry}})$, $d\mathrm{O}_{3,\,+\mathrm{Chemistry}}/d\mathrm{T}$, and $d\mathrm{O}_{3,\,\mathrm{Transport}}/d\mathrm{T}$.

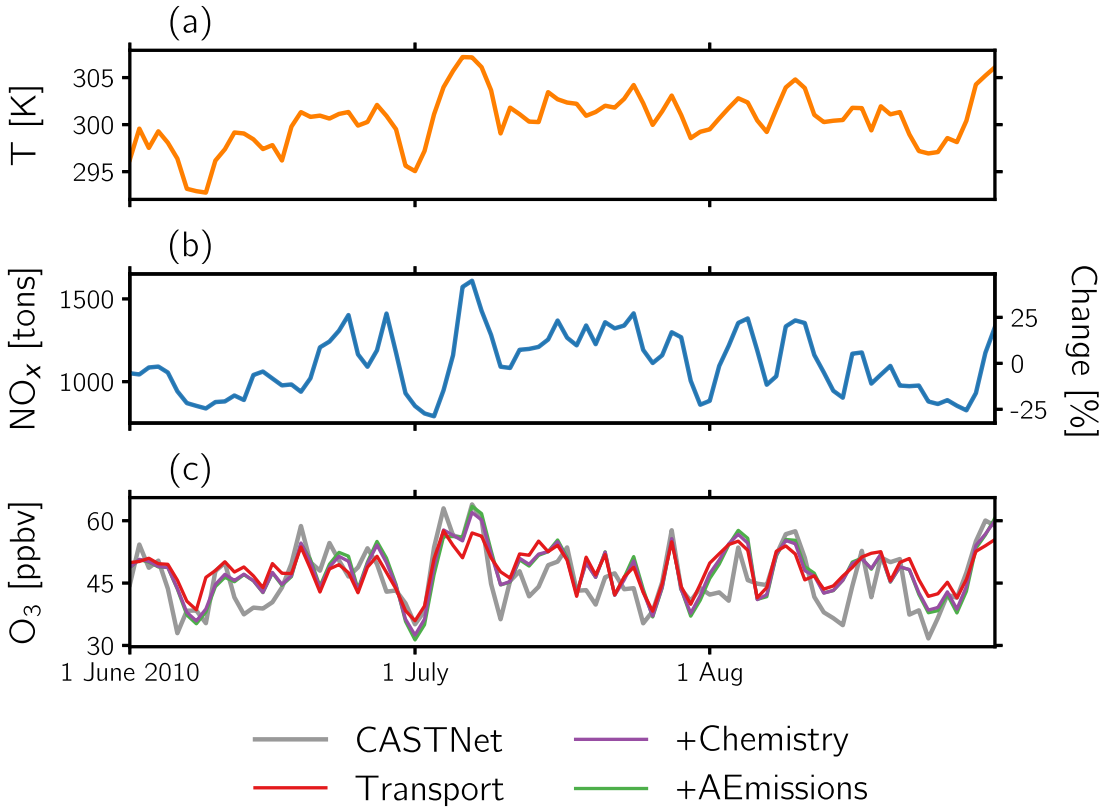

Figure 5. (a) Afternoon MERRA-2 2-meter temperature averaged over grid cells co-located with observational sites in the Northeast; (b) Northeast-summed anthropogenic NO_x emissions measured by Continuous Emissions Monitoring Systems (CEMS; Figure S1); (c) afternoon observed O_3 averaged over observational sites in the Northeast and O_3 from three CTM sensitivity simulations averaged over all grid cells in the Northeast. (a-c) represent daily values for summer 2010, and the states included in the Northeast are outlined in Figure 1.

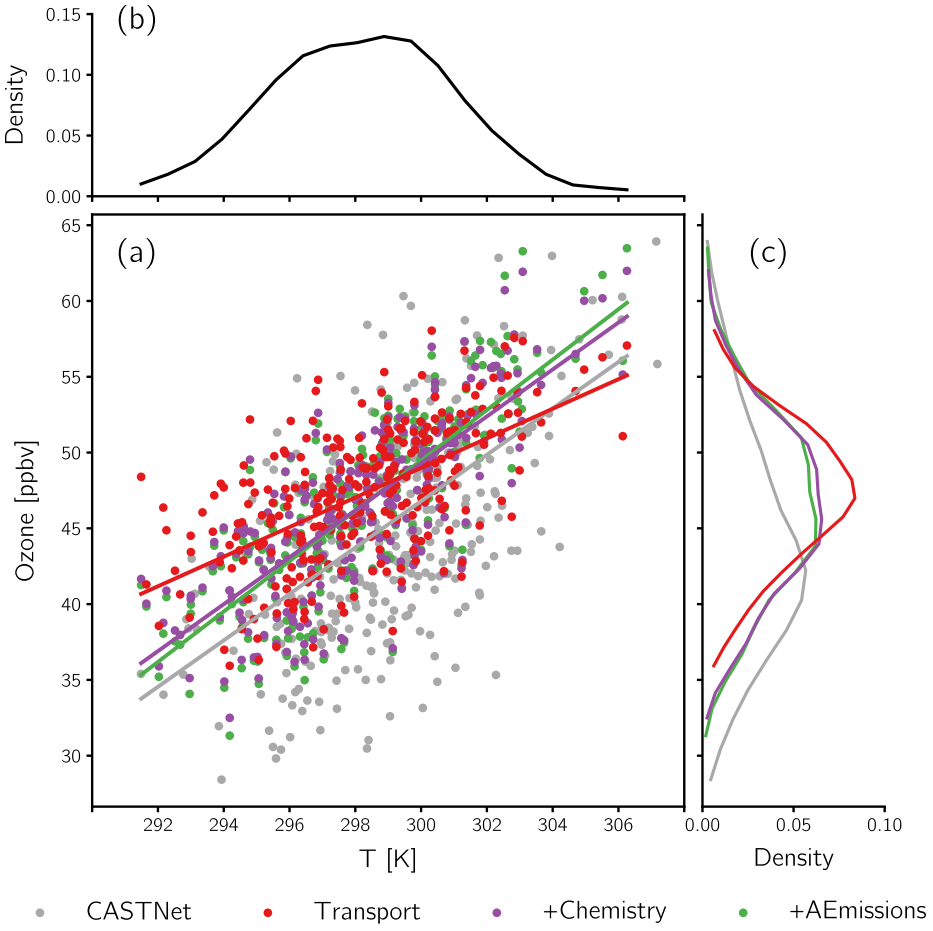

Figure 6. (a) Scatterpoints show Northeast-averaged daily afternoon O_3 from observations and CTM sensitivity simulations versus temperature. Lines are the OLS linear regressions fit through the data. (b) Kernel density estimate (KDE) of temperature and (c) KDEs of observed and simulated O_3.

Table 2. Summary of results in the Northeastern U.S. (outlined region in Figure 1) determined with regionally-averaged quantities.

	μ [ppbv]	σ [ppbv]	$O_{3,\,P_{90}} - O_{3,\,P_{50}}$ [ppbv]	$O_{3,\,P_{10}} - O_{3,\,P_{50}}$ [ppbv]	$O_3(T_{P_{90}}) - O_3(T_{P_{50}})$ [ppbv]	$O_3(T_{P_{10}}) - O_3(T_{P_{50}})$ [ppbv]	dO_3/dT [ppbv K^{-1}]
Transport	47.262	4.517	5.267	-6.142	5.252	-3.864	0.976
+Chemistry	46.553	5.535	7.019	-7.436	8.746	-6.229	1.549
+AEmissions	46.549	5.831	7.094	-7.809	9.485	-6.601	1.662
CASTNet	44.089	7.164	11.025	-7.854	10.424	-4.329	1.553

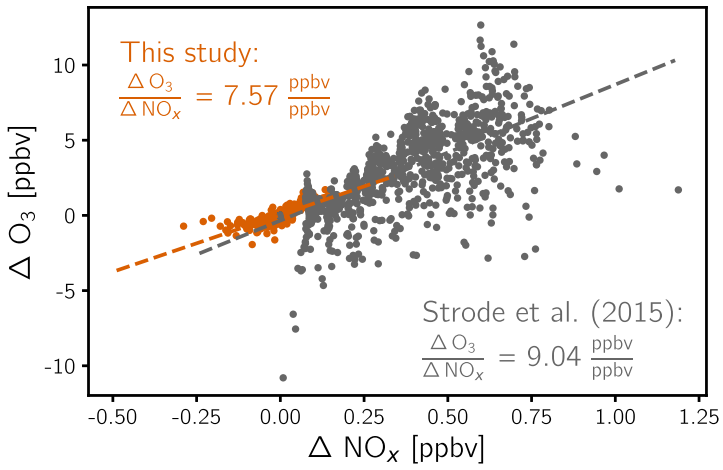

Figure 7. Northeast-averaged absolute changes of daily afternoon O_3 versus absolute changes of NO_x. For this study the change (i.e., Δ) corresponds to the difference between the +AEmissions and +Chemistry simulations for summers 2008-2010. For Strode et al. (2015), Δ refers to the daily change between the EmFix and Std simulations for summers 2000-2010. $\Delta\, O_3\, \Delta\, NO_x^{-1}$ is calculated using OLS linear regression.

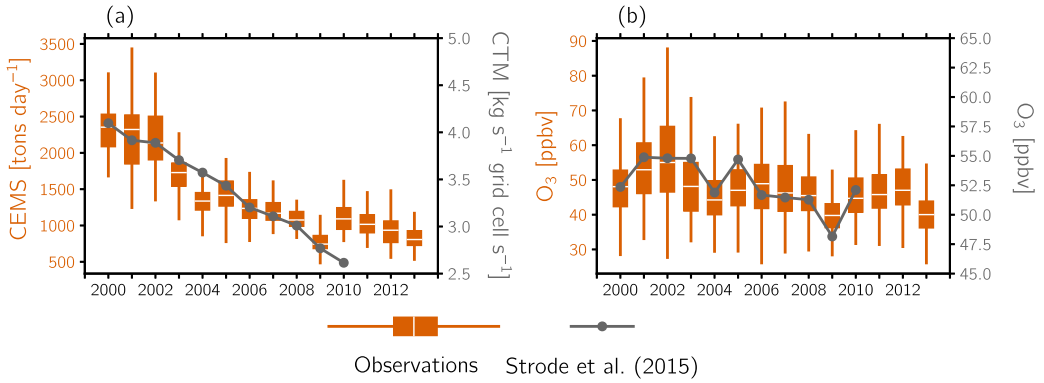

Figure 8. Summer (a) Northeast-summed daily anthropogenic NO_x emissions from CEMS (boxplots) and Northeast-averaged NO from the emissions inventory of the Std simulation of the CTM (timeseries) and (b) Northeast-averaged observed O_3 from CASTNet (boxplots) and modeled O_3 from Std simulation (time series). Center white lines in boxplots correspond to median summer values, and whiskers extend to 1.5 × IQR.

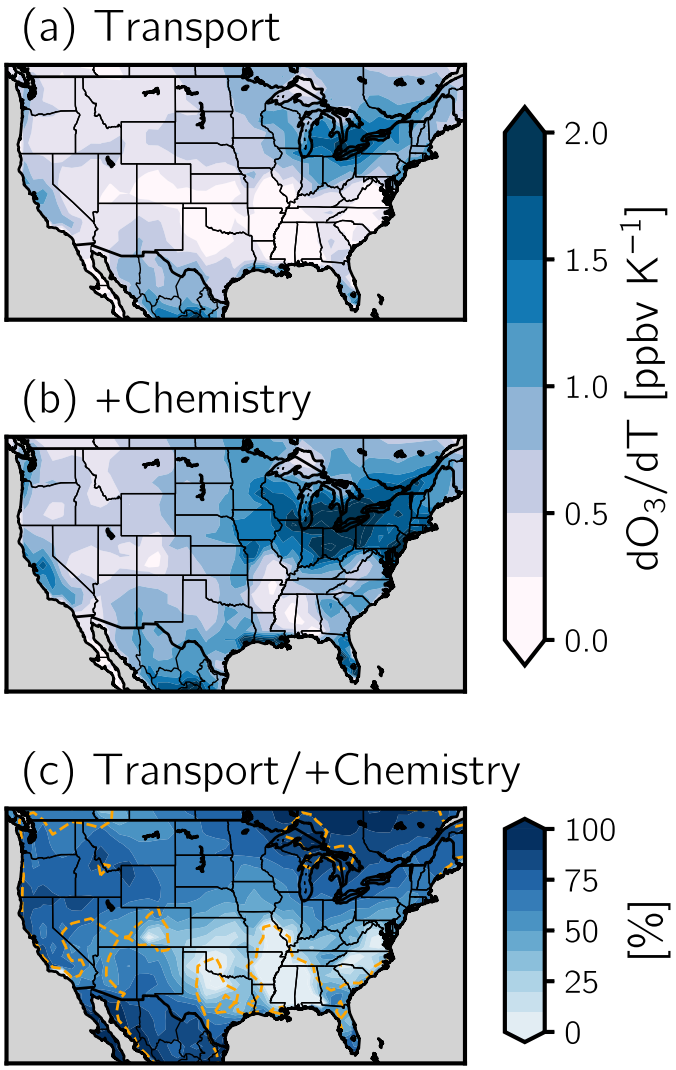

811 **Figure 9.** $d\mathrm{O_3}/d\mathrm{T}$ in the (a) Transport and (b) +Chemistry simulations. (c) The quotient of
812 each simulation's $d\mathrm{O_3}/d\mathrm{T}$ multiplied by 100; a value of 100% implies that the $\mathrm{O_{3,\,P_{90}}}$ magnitude
813 did not change between simulations. Orange contours enclose regions where $r(\mathrm{T}, \mathrm{O_3}) < 0.4$.

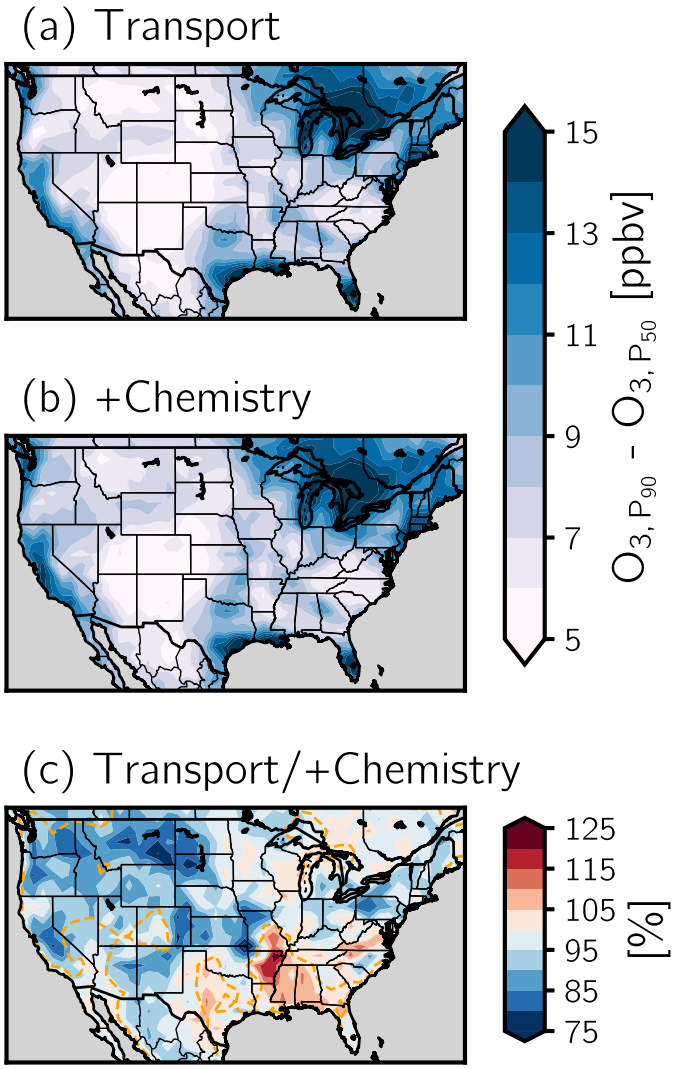

814 **Figure 10.** O_3 enhancements for high O_3 events ($O_{3,\,P_{90}} - O_{3,P_{50}}$) in the (a) Transport and
815 (b) +Chemistry simulations. (c) The ratio of the enhancements from each simulation converted
816 to percents, where the ratio is given by $(O_{3,\,P_{90}} - O_{3,P_{50}})_{\text{Transport}}/(O_{3,\,P_{90}} - O_{3,P_{50}})_{\text{+Chemistry}}$.
817 Orange contours enclose regions where $r(\mathrm{T}, \mathrm{O_3}) < 0.4$.

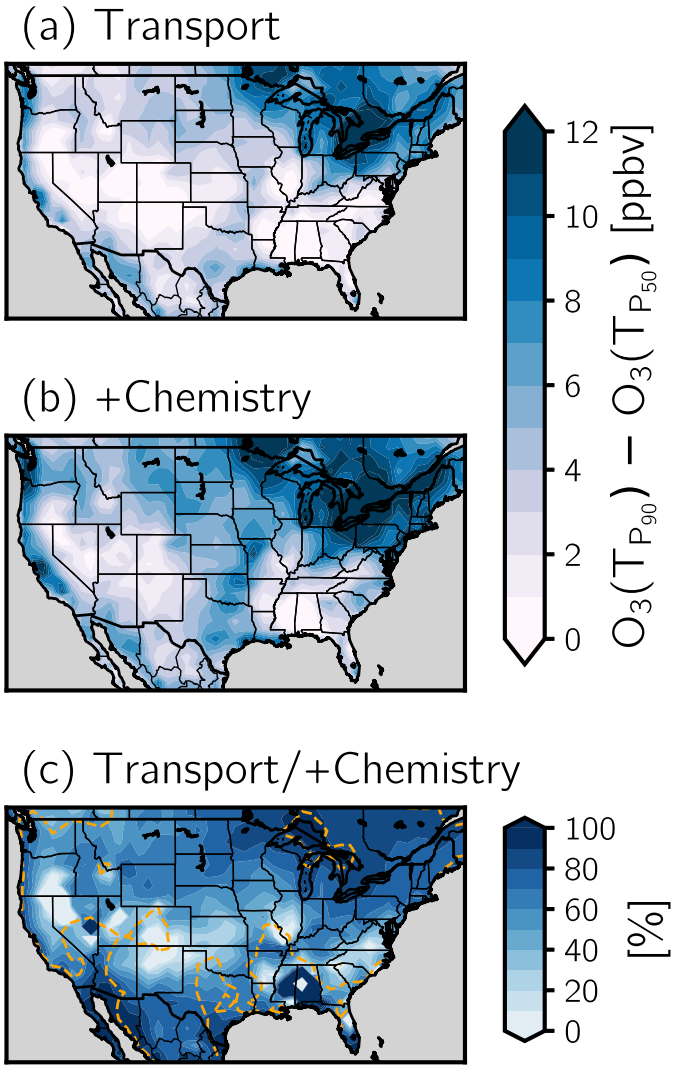

818 **Figure 11.** Same as Figure 10 but showing O_3 enhancements on hot days: $O_3(T_{P_{90}})$ –
819 $O_3(T_{P_{50}})$.